The Astrophysical Journal, 791:102 (11pp), 2014 August 20 doi:10.1088/0004-637X/791/2/102

INSTABILITY OF THE HELIOPAUSE DRIVEN BY CHARGE EXCHANGE INTERACTIONS

K. Avinash[1,2], G. P. Zank[1,3], B. Dasgupta[1], and Shikha Bhadoria[2]
[1] Center for Space Plasma and Aeronomic Research (CSPAR), University of Alabama in Huntsville, Huntsville, AL 35805, USA
[2] Department of Physics and Astrophysics, University of Delhi, Delhi, 110007, India
[3] Department of Space Science, University of Alabama in Huntsville, Huntsville, AL 35899, USA
Received 2014 March 21; accepted 2014 June 23; published 2014 August 1

ABSTRACT

The stability of the heliopause that separates the tenuous hot magnetized heliosheath plasma from the dense cool local interstellar magnetized plasma is examined using a fully general model that includes all the essential physical processes. Charge exchange coupling between plasma protons and primary interstellar neutral atoms provides an effective gravity that drives Rayleigh–Taylor (RT)-like instabilities. The velocity difference or shear between the heliosheath and interstellar flows, when coupled to energetic neutral atoms (ENAs), drives a Kelvin–Helmholtz (KH)-like instability on the heliopause. The shoulder region of the heliopause is unstable to a new instability that has characteristics of a mixed RT–KH-like mode. The instabilities are not stabilized by typical values of the magnetic fields in the inner and outer heliosheath (OHS). ENAs play an essential role in driving the KH-like instability, which is fully stabilized in their absence by magnetic fields. The nonlinear phase of these instabilities is briefly discussed. We also discuss the possibility that RT-like or mixed KH–RT-like instabilities drag outer heliosheath/very local interstellar medium (OHS/VLISM) magnetic field lines into the inner heliosheath (IHS) with the VLISM flow, and the possibility that IHS and VLISM magnetic field lines experience reconnection. Such reconnection may (1) greatly enhance the mixing of plasmas across the heliopause and (2) provide open magnetic field lines that allow easy ingress of galactic cosmic rays into the heliosphere and corresponding easy loss of anomalous cosmic rays from the heliosphere.

Key words: instabilities – ISM: magnetic fields – local interstellar matter – magnetic fields – magnetic reconnection – Sun: heliosphere

Online-only material: color figures

1. INTRODUCTION

The heliopause (HP) is a surface that separates the high temperature, tenuous solar wind (SW) plasma in the inner heliosheath (IHS) from the relatively dense, cooler, plasma of the local interstellar medium (LISM) in the outer heliosheath (OHS). Across the HP, the pressure of the plasma within the heliosphere balances the pressure of the surrounding interstellar medium (Fahr et al. 1986). In general, we expect the HP to lie between 120–150 AU from the Sun in the direction of the motion of Sun with respect to the interstellar medium. The HP has now been crossed by the *Voyager 1* spacecraft (Gurnett et al. 2013; Burlaga et al. 2013) at 125 AU and the magnetic fields on either side are approximately parallel along the surface of the HP. The thickness of the HP could range from a fraction of an AU to approximately 10 AU (Fahr et al. 1986).

In magnetohydrodynamic (MHD) models, the HP is a sharp tangential discontinuity (TD) that prevents the mixing of the hot SW plasma and the cool LISM plasma. The interstellar neutral hydrogen, being uncharged, passes through the HP and experiences resonant charge exchange interactions with the plasma, slowing down the SW and heating the plasma in the IHS. The energetic neutrals in the IHS created in these interactions, called secondary neutrals or energetic neutral atoms (ENAs; Gruntman 1992; Gruntman et al. 2001) propagate upstream into the OHS across the HP. These secondary neutrals or ENAs cause charge exchange interactions with the ions in the OHS, causing significant heating of the OHS plasma (Zank et al. 1996, 2001, 2013).

Results from a number of time-dependent hydromagnetic simulations of the global HP have emphasized the importance of resonant charge exchange interactions between LISM neutrals and SW plasma in determining the steady as well as the dynamic properties of the heliosphere (Baranov & Malama 1993; Pauls et al. 1995; Liewer et al. 1996; Zank et al. 1996). Multi-fluid simulations by Zank et al. (1996) and Liewer et al. (1996), and later by Florinski et al. (2005) and Borovikov et al. (2008) have shown that on account of the friction between the neutral hydrogen from LISM and the plasma ions, mediated by resonant change exchange collisions, the HP may be potentially unstable to large-scale modes. Zank (1999a) showed that frictional drag between the plasma and neutral H in the vicinity of the HP would drive a Rayleigh–Taylor (RT)-like instability. Subsequent simulations confirmed the existence of an RT-like instability caused by charge exchange between the primary neutrals from the LISM (or OHS) and SW ions. In particular, the high-resolution simulations of Borovikov et al. (2008) have identified two types of unstable modes in the vicinity of HP; an RT-like mode driven mainly by the charge exchange between neutrals and plasma ions and an RT–KH-like mixed mode, driven by the combination of charge exchange and plasma flow shear across HP. The charge exchange interaction introduces an effective gravitational forceacting on the plasma in the direction of the flow of the LISM neutrals, which flow downstream from the OHS to the IHS. The plasma density gradient is in the opposite direction because the LISM plasma is much denser than the SW plasma. Hence, RT-like modes are expected to be unstable in the neighborhood of the nose region of the HP, where the effective gravitational force and the plasma density gradient are nearly in the opposite direction. The plasma flows on the other hand, which are weak in the vicinity of the nose region, are strong on the flanks with significant shear across the HP.

Hence, the Kelvin–Helmholtz (KH) modes are expected to be unstable on the flanks of the HP. Such scenarios were considered by several authors. The early investigation of Fahr et al. (1986) discussed the problem of plasma mixing between the SW and the ambient ionized component of the very local interstellar medium (VLISM). Fahr et al. suggested that the HP should not be treated as a clearly defined surface that separated the shocked SW plasma from the VLISM plasma. Instead, Fahr et al. (1986) suggested that the HP should be an extended transition layer with stationary or turbulent plasma properties, depending on the specific plasma condition on the interstellar side. For weak VLISM magnetic field $<10^{-7}$ G, Fahr et al. suggest that the width of the transition region is likely to be determined by standard hydromagnetic RT or KH instabilities developing in the adjacent plasma flows. The resulting plasma mixing rates at the HP may be 20%–30% of the impinging plasma flow. By analogy with planetary magnetopauses, Fahr et al. (1986) estimated that for VLISM magnetic fields $\sim 10^{-6}$ G or larger, magnetic field reconnection processes might play a dominant role in the plasma mixing, which can be 10% of the impinging flow across the HP. The possibility that interstellar neutrals may be responsible for the destabilization of the HP was not discussed in this work. Baranov et al. (1992) investigated the KH instability in the flank region of the HP using a linear perturbation analysis (equivalent to a first-order WKB method) for compressible flows. Chalov (1994) considered the instability of a TD in plasma with cosmic rays and its application to the HP. This was also investigated in more detail by Zakharian et al. (1998). Ruderman (2000) and Ruderman et al. (2004) studied the absolute and convective properties of the KH instability of the HP, treated as a TD with viscosity. Recent high-resolution numerical simulations (Borovikov et al. 2008) show that strong instabilities develop both near the nose of the HP as well as in the flank regions. More importantly, the simulations show that the KH instability of the flanks, which is stabilized by the magnetic fields that are present in the in IHS and OHS, is resuscitated by ENAs.

The charge exchange interaction introduces momentum and energy sources in the plasma dynamics and thus introduces significant changes in the dynamics of the system. Zank (1999a, 1999b) derived a modification of the plasma incompressibility condition due to charge exchange in the heliosphere and formulated the problem of the stability of the HP in terms of the charge exchange modified plasma incompressibility condition. This condition is based on the theory of nearly incompressible hydrodynamics developed earlier by Zank & Matthaeus (1991). Later, a more detailed numerical and analytic analysis of the RT instability for an axisymmetric heliosphere in the vicinity of the nose region, using the charge exchange modified plasma incompressibility condition was given by Florinski et al. (2005).

In this paper, we study the stability of modes localized in the vicinity of HP. Our analysis includes a number of effects that are important in the heliosphere. In addition to resonant charge exchange with primary neutrals from LISM, we have also taken into account the effects of magnetic fields, plasma flows, and ENAs. Plasma flows and flow shear are significant in the flanks of HP and hence can play an important role in the stability of HP flanks. The effect of magnetic fields is important because it is well known from the work of Chandrasekhar (1981) that magnetic fields can significantly change the stability thresholds of RT and KH instabilities. There is considerable uncertainty in the estimates of the magnitude and the direction of the magnetic field in the vicinity of HP. The results of Burlaga et al. (2013), when interpreted now in the light of the crossing of the HP as identified by Gurnett et al. (2013), suggest that the magnetic fields on either side of the HP are approximately parallel, with perhaps a change in orientation. We present a full, general analysis below and then consider the magnetic field parameters and densities suggested by the *Voyager 1* magnetometer and wave instrument measurements. One of the main effects of the interstellar magnetic field is that it introduces a north–south asymmetry in the heliosphere as is evident by the *Voyager* crossings of the termination shock (TS). Estimates by Heerikhuisen & Pogorelov (2011), based on the numerical modeling of the *IBEX* observation of the enhanced ENA flux, constrain the field to be <3 μG (see also Strumik et al. 2011; Zank et al. 2013; Ben-Jaffel et al. 2013). The effects of ENAs are important because, as stated earlier, recent simulations by Borovikov et al. (2008) have shown that the presence of ENAs is essential for destabilizing the flanks. This has been confirmed again by Borovikov & Pogorelov (2014), who showed that solar cycle variation can provide the perturbative trigger that initiates instabilities on the HP. As the heliosphere is asymmetric, we carry out a stability analysis in a local reference frame located on the HP. This model is applicable to the entire HP, i.e., close to the nose, flanks and the shoulder region in between. In the neighborhood of the nose where plasma flows are weak, it generalizes the earlier analyses of Zank (1999a) and Florinski et al. (2005) to include the effect of the magnetic field in the IHS and OHS. The general dispersion relation (DR) shows that in the relevant parameter space of the heliosphere and LISM, the HP is indeed unstable to RT-like modes in the vicinity of the nose, and a new mixed RT–KH-like mode in the shoulder region of HP is found. The role of ENAs vis-a-vis primary cold neutrals is interesting in our model. On account of the effective gravity, the primary neutrals destabilize the RT-like mode in the nose region and stabilize the KH mode in the flanks (Zank 1999a). In contrast, due to counter streaming, ENAs stabilize the RT-like modes in the nose region and destabilize the KH-like modes in the flanks. Thus, our DR shows that in the absence of ENAs and magnetic fields, the flanks are unstable to KH modes. These modes are stabilized by the magnetic fields parallel to the HP in the IHS and OHS. However, this stabilization by magnetic fields is annulled and the KH-like instability is fully resuscitated by the presence of ENAs. These results are consistent with simulations of Borovikov et al. (2008).

The paper is organized as follows. In Section 2, we discuss the basic equation of our model. In Section 3, we derive the DR and discuss the linear stability of the HP in various regions. In Section 4, we discuss nonlinear stability of the various excited modes, and, in the last section, we provide a summary and discuss the conceptual effect of the RT-like and mixed RT–KH-like instabilities on the magnetic fields in the IHS and OHS.

2. GOVERNING EQUATIONS OF THE MODEL

The description of the plasma flow and its interaction with neutral hydrogen via the resonant charge exchange interaction is described by the following set of equations:

$$\frac{\partial \rho}{\partial t} + \nabla \cdot (\rho \mathbf{u}) = 0, \tag{1}$$

$$\rho \left(\frac{\partial \mathbf{u}}{\partial t} + \mathbf{u} \cdot \nabla \mathbf{u} \right) + \nabla p = \frac{1}{c} \mathbf{J} \times \mathbf{B} - \nu_p \rho (\mathbf{u} - \mathbf{V}_p) - \nu_s \rho (\mathbf{u} - \mathbf{V}_s), \tag{2}$$

$$\frac{\partial p}{\partial t} + \mathbf{u}\cdot\nabla p + \gamma p \nabla\cdot\mathbf{u} = \nu_p \rho\left(\frac{\gamma-1}{2}(\mathbf{u}-\mathbf{V}_p)^2 + \frac{kT_p}{m_H} - \frac{p}{2\rho}\right) + \nu_s \rho\left(\frac{\gamma-1}{2}(\mathbf{u}-\mathbf{V}_s)^2 + \frac{kT_s}{m_H} - \frac{p}{2\rho}\right), \quad (3)$$

$$\frac{\partial N_\alpha}{\partial t} + \nabla\cdot(N_\alpha \mathbf{V}_\alpha) = -\nu_\alpha \frac{\rho}{m_H}, \quad (4)$$

$$\nabla\times\mathbf{B} = \frac{4\pi}{c}\mathbf{J}. \quad (5)$$

In these equations ρ, $\mathbf{u}$, p, and J are the plasma mass density, velocity, pressure, and current density, respectively, $\mathbf{B}$ is the magnetic field, and $\gamma = 5/3$ is the specific heat ratio. The charge exchange interaction introduces sources and sinks in the momentum and energy equations which appear on the right-hand side (RHS) of Equations (2)–(4); Holzer 1972; Zank 1999b). Since the number of ions is conserved in this interaction, there are no such terms in the continuity equation. In our analysis, we consider two populations of neutrals: primary neutrals from the LISM, which are relatively cooler and denser ($T_p \sim 10^4$ K), and ENAs or secondary hot and rarer neutrals ($T_s \sim 10^6$ K) from the IHS, created by the charge exchange of primary neutrals with the hot plasma in the IHS (Zank et al. 1996, 2013; Heerikhuisen et al. 2006). These neutrals undergo further change exchange interactions in the IHS and OHS. It should be noted that the bulk ENA distributions are not Maxwellian, of course, and the above temperature should be interpreted as an average of effective temperatures of ENAs produced by charge exchange with core SW ions and with much hotter pickup ions (PUIs; Malama et al. 2006; Heerikhuisen et al. 2006, 2008; Zank et al. 2010). The density, velocity, and charge exchange frequency of these two populations of neutrals is denoted by N_α, $\mathbf{V}_\alpha$ and ν_α, respectively (where $\alpha = p, s$). The charge exchange frequency is given by the expression $\nu = \sigma U^* N$, where $\sigma = 3\times10^{-15}$ cm^2 is the charge exchange interaction cross section (Lindsay & Stebbings 2005) and the speed U^* is the characteristic interaction speed between protons and neutrals. The exact expression for U^* is given in Pauls et al. (1995), their Equation (A.14), and is proportional to the square root of the sum of the squares of the neutral H and proton thermal speeds and the bulk velocity difference between the proton and neutral H distributions, respectively. As discussed in the Appendix of Florinski et al. (2005), a good approximation is that U^* is typically 1.5 times the thermal speed of hot neutrals. The neutral velocity in this set of equations is usually taken to be constant so that an equation of motion for the neutral component is not required. Since the neutral H charge exchange mean free path greatly exceeds 50 AU in the vicinity of the HP, a constant neutral velocity is reasonable. This greatly simplifies the analysis while still retaining the essential features of the plasma–neutral charge exchange interaction. The key point in the model of Zank (1999a) is the modification of the incompressibility condition due to charge exchange, which is given by

$$\nabla\cdot\mathbf{u} = -\frac{\nu}{2\gamma}. \quad (6)$$

The condition (Equation (6)) replaces the usual plasma incompressibility condition of standard hydrodynamics. The justification of this condition, in the case of primary neutrals, relies on the fact that in the subsonic heliosheath, the term $p/2\rho$, which is roughly proportional to the plasma thermal speed, is large and hence may be retained in comparison to terms that depend on the bulk and thermal speeds of neutrals. The nearly incompressibility condition in Equation (6) also requires that $\mathbf{u}\cdot\nabla p \ll \gamma p\nabla\cdot\mathbf{u}$. This is justified as variations in the pressure in the heliosheath between TS and HP are small, i.e., the compressibility is small. Subsequently, the effect of secondary hot neutrals (ENAs) on the RT-like and KH-like instability was considered by Florinski et al. (2005) and Dasgupta et al. (2006). These authors retained the term dependent on the thermal speed of hot neutrals in the OHS. However, their model shows a damping effect of ENAs on the HP instability, which is not consistent with the simulations of Borovikov et al. (2008). In this paper, we reexamine the relative importance of various terms on the RHS of Equation (3) in the IHS and OHS. Typically, in the close neighborhood of the HP, the plasma temperature (proportional to $p/2\rho$) varies from $\sim5\times10^5$ K along flanks to $\sim10^6$ K at the nose in the IHS (Borovikov et al. 2008). The temperature of ENAs also lies in a similar range. As discussed in detail by Zank et al. (1996, 2013), when hot neutrals propagate upstream into the OHS, they cause significant heating of the plasma in the OHS due to secondary charge exchange with LISM protons. To ensure that this effect is properly captured, we estimate the plasma temperature in the OHS using the results of the multi-fluid (i.e., plasma plus three neutral H gases) model of Zank et al. (1996) and a kinetic model (Zank et al. 2013), which account for the heating of OHS due to ENAs. The plasma temperature is typically $\sim5\times10^4$ K. The primary neutral density in the OHS is $N_p \sim 0.2$ cm^{-3} while the ratio of primary to secondary hot neutral H atoms is typically $N_s/N_p \sim 0.01$ (Zank et al. 1996; Heerikhuisen et al. 2006). We first consider the IHS. On assigning the indices h (heliospheric) and i (interstellar) for IHS and OHS variables, respectively, we have in the first parenthesis on the RHS of Equation (3), $(p/2\rho)_h \simeq 10^6$ K, $T_p \simeq 10^4$ K, and $V_p \sim 25$ km s^{-1}, hence the third term is the largest, as first pointed out by Zank (1999a). This is also bigger than all the terms in the second parenthesis as $\nu_{sh}/\nu_{ph} < 1$. In the OHS, the plasma term is 5×10^4 K, hence it is still the largest term in the first parenthesis (Florinski et al. 2005). In the second parenthesis, the second term proportional to $T_s \sim 5\times10^5$–10^6 K is the largest, but, since $(kT_s/m_{\rm H})/(p/2\rho)_i \sim 10$–$20$ and $\nu_{si}/\nu_{pi} \sim 0.01$–$0.05$, $\nu_p(p/2\rho)_i$ is still greater than $\nu_s(kT_s/m_{\rm H})$ and hence it is the largest term on the RHS of Equation (3). Thus, in both the IHS and OHS, the charge exchange modified incompressibility condition becomes

$$\nabla\cdot\mathbf{u} = -\frac{\nu_p}{2\gamma}. \quad (7)$$

This is consistent with the original condition suggested by Zank (1999a) and is different from Florinski et al. (2005) and Dasgupta et al. (2006) who retain the hot neutral thermal velocity term in the OHS. It should be noted that in our model, the effect of ENAs is still retained in the momentum conservation equation in Equation (2).

The HP boundary can be roughly divided into three regions: the nose region where the interstellar plasma and the SW plasma flows stagnate against each other and the resulting plasma flows are weak, the flank regions away from the nose region with significant plasma flow and flow shear across the HP, and the shoulder region between the flanks and nose. From the nose region, the plasma flow on either side of HP is diverted toward the flanks. Thus, the plasma flow is along the HP surface while the flow shear and the plasma density gradient are perpendicular

to it. The primary neutrals from the LISM flow unhindered across the HP. In the nose region, the neutral flow is in the direction opposite to that of the SW plasma flow. The angle θ between the two flows gradually decreases from 180° along the HP to nearly 0° on the flanks where both flows are nearly in the same direction. The ENAs on the other hand, which are generated in the heliosheath, propagate upstream from the IHS, in a direction roughly perpendicular to the HP everywhere.

Since the heliosphere is asymmetric by virtue of the LISM magnetic field, the assumption of axisymmetry used in many earlier simulations becomes invalid. In such cases, it is convenient to carry out the analysis in a local reference frame. Hence, we describe the HP equilibrium in a planar geometry with the origin of the local reference frame located on the HP boundary. In this frame, the z-axis is perpendicular while the x–y plane is tangent to the HP surface. The SW flow is in the region $z < 0$ and the interstellar plasma flow is in the region $z > 0$. The x-axis is assumed to be aligned along the equilibrium plasma flow velocity $\mathbf{u}_0 = (u, 0, 0)$ while the flow shear and plasma density gradient are along the z-axis across the HP. The primary neutrals move downstream across the HP boundary in the x–z plane with a constant speed $\mathbf{V}_p$. Let θ be the angle between the z-axis and $\mathbf{V}_p$. Along the HP boundary, this angle changes, being close to 180° in the nose region and nearly 90° in the flank region. The ENAs, on the other hand, move upstream across the HP at an angle Ψ from the local z-axis, which remains close to zero everywhere along the HP boundary.

Next, we consider the effect of the magnetic field. In our model, we consider the magnetic field to be draped on the HP surface. As shown below, this is a reasonable assumption which has been included in recent simulations of the HP and may have been observed in the *Voyager 1* magnetic field measurements. The diffusion of magnetic field in the plasma is governed by the equation

$$\frac{\partial \mathbf{B}}{\partial t} = \frac{\eta c^2}{4\pi}\nabla^2 \mathbf{B}, \tag{8}$$

where η is the plasma resistivity. The magnetic field diffusion time is given by $\tau_d \simeq 4\pi L^2/\eta c^2$ where L is the scale length of B variation. In order to estimate τ_d, we need the value of η. Since the LISM neutral density is much higher that of the ENAs, it will be determined primarily by electron collisions with primary neutrals, denoted by η_{en}. In addition, there will be the usual *Spitzer* resistivity η_S due to the electron–ion collisions. The expressions for η_{en} and η_S are given by

$$\eta_{en} = 2.5 \times 10^{-3} T_e^{1/2} \frac{N_p}{n}\sigma, \quad \eta_S = 7.3 \times 10^{-9} \frac{z \ln \Delta}{T_e^{3/2}}, \tag{9}$$

where $\sigma = 3 \times 10^{-15}$ cm^{-2} is the electron–neutral collision cross section, z is the atomic number, T_e is the electron temperature in kelvins, n is the plasma number density, and $\ln \Delta \simeq 20$ is the Coulomb logarithm. In the nose region, the typical parameters for the OHS are $n \sim 0.3$ cm^{-3}, $N_p \simeq 0.2$ cm^{-3}, $T_e = 10^4$ K. For these parameters, $\eta_S \simeq 10^{-13}$ s, which is bigger than $\eta_{en} \simeq 10^{-15}$ s. On the other hand, in the IHS with hotter and rarer plasma $n \simeq 0.005$ cm^{-3}, $T_e = 10^6$ K, and the electron–neutral resistivity is $\eta_{en} \simeq 10^{-13}$ s, which dominates $\eta_S \simeq 10^{-16}$ s. On the flanks of the OHS with $n \simeq 0.025$ cm^{-3}, $N_s \simeq 0.04$ cm^{-3}, $T_e = 5 \times 10^4$ K, $\eta_S \simeq \eta_{en} \simeq 10^{-14}$ s. On the other hand, in the IHS in this region with $n \simeq 0.003$ cm^{-3}, $T_e = 5 \times 10^5$ K, $\eta_{en} \simeq 5 \times 10^{-14}$ s, which dominates $\eta_S \simeq 5 \times 10^{-16}$ s. These estimates show that in the IHS the resistivity is determined mainly by electron–neutral collisions η_{en} and is typically in the range 10^{-14}–10^{-13} s, while in the OHS it is primarily the *Spitzer* resistivity that is important since it lies in a similar range. These estimates implicitly assume that the plasma in the vicinity of the HP is quiescent. However, the plasma in the vicinity of the HP is more likely to be turbulent. This turbulence could be driven by strong plasma flows and flow shear, which exist in the vicinity of the HP or alternatively by RT-like modes driven by a combination of charge exchange induced effective gravity and plasma density gradients across the HP. In fact, the DR derived in this paper shows that for typical parameters, the threshold for these instabilities is crossed. Hence, the plasma close to the HP is most likely to be turbulent. This turbulence causes an anomalous enhancement in the collision frequency and the resistivity by a factor $1/g$ (Ichimaru 1973; Ershkovich & Mendis 1983) where $g = (n\lambda_d^3)^{-1}$ is the plasma parameter and λ_d is the plasma Debye length. For typical HP parameters, $1/g \simeq 10^{11}$ so that $\eta \simeq 10^{-2}$–10^{-3} s. Then, with a scale length L roughly equal to the width of the HP boundary ~10 AU, the magnetic diffusion time $\tau_d \simeq 10^{10}$–10^{11} s. This is still larger by two to three orders of magnitude than the typical HP instability time scale of 10–50 yr seen in the numerical simulations. These estimates thus show that the plasma in the vicinity of the HP is nearly ideal, i.e., $\eta \simeq 0$, and hence the magnetic field will not diffuse into the heliosphere, but will instead drape around it. In this case, the magnetic field $\mathbf{B}$ will lie on the HP surface in the x–y plane. Since the plasma in the vicinity of HP is nearly ideal, the evolution of $\mathbf{B}$ is governed by the equation

$$\frac{\partial \mathbf{B}}{\partial t} = \nabla \times \mathbf{u} \times \mathbf{B}. \tag{10}$$

The equation describing the zero-order equilibrium HP in the presence of two types of neutral H (denoted by the subscripts p and s for primary and secondary) is obtained by taking the z component of the zero-order momentum equation, and is given by

$$\frac{\partial}{\partial z}\left(p + \frac{B^2}{8\pi}\right) = (\nu_p V_{pz} + \nu_s V_{sz})\rho, \tag{11}$$

where the zero-order pressure, p, and magnetic field, $\mathbf{B}$, only depend on the z coordinate.

3. STABILITY OF THE HELIOPAUSE BOUNDARY

In this section, we examine the stability of the HP. The plasma continuity equation is given by

$$\frac{\partial \rho}{\partial t} + \mathbf{u} \cdot \nabla \rho = \frac{\nu_p}{2\gamma}\rho, \tag{12}$$

where we have eliminated the divergence of the flow velocity through Equation (7). In our stability analysis, instead of using the full energy equation given in Equation (3), we will use the incompressibility condition given in Equation (7) as the equation of state to calculate the pressure.

Since the HP may be regarded as a TD at $z = 0$ in our coordinate system, the stability problem constitutes an expansion in terms of singular perturbations. The equations are solved across and away from the singular surface and the solutions are asymptotically matched to obtain the eigenvalue. For the stability analysis, we will consider a simple plasma density and flow profile, which is constant in the IHS and in the OHS, i.e., ρ_h = constant, $\mathbf{u}_h$ = constant in $z < 0$ and

ρ_i = constant, $\mathbf{u}_i$ = constant in $z > 0$, with a jump across the TD at $z = 0$. The density, pressure, magnetic field, and velocity are perturbed as $\rho + \delta\rho$, $p + \delta p$, $\mathbf{B} + \delta\mathbf{B}$, and $\mathbf{u} + \delta\mathbf{u}$, respectively. With these perturbations, the set of linearized equations for the stability analysis is

$$\frac{\partial \delta\rho}{\partial t} + \mathbf{u}\cdot\nabla\delta\rho + \delta w\frac{d\rho}{dz} = \frac{\nu_p}{2\gamma}\delta\rho, \tag{13}$$

$$\rho\frac{\partial \delta\mathbf{u}}{\partial t} + \rho\delta\mathbf{u}\cdot\nabla\mathbf{u} + \delta\rho\mathbf{u}\cdot\nabla\mathbf{u} + \rho\mathbf{u}\cdot\nabla\delta\mathbf{u} + \nabla\left(\delta p + \frac{\delta\mathbf{B}\cdot\mathbf{B}}{4\pi}\right) = \frac{\mathbf{B}\cdot\nabla\delta\mathbf{B}}{4\pi} - \nu_p(\mathbf{u}-\mathbf{V}_p)\delta\rho - \nu_p\rho\delta\mathbf{u} - \nu_s(\mathbf{u}-\mathbf{V}_s)\delta\rho - \nu_s\rho\delta\mathbf{u}, \tag{14}$$

$$\nabla\cdot\delta\mathbf{u} = 0 = \nabla\cdot\delta\mathbf{B}, \tag{15}$$

$$\frac{\partial \delta\mathbf{B}}{\partial t} = \nabla\times\delta\mathbf{u}\times\mathbf{B} + \nabla\times\mathbf{u}\times\delta\mathbf{B}, \tag{16}$$

where δw is the z component of the perturbed plasma velocity. For the stability analysis, we consider the eigenfunction $f(z)\exp[nt + \mathbf{k}\cdot\mathbf{r}]$, which represents propagating waves on the singular surface in the x–y plane $\mathbf{k} = (k_x, k_y)$. Next, we consider the boundary conditions at the perturbed HP surface. The unperturbed HP surface is given by $z = 0$. Let ζ be the perturbation of this surface. Then, we have

$$\left(\frac{\partial}{\partial t} + \mathbf{u}\cdot\nabla\right)\zeta = \delta w. \tag{17}$$

From this equation we obtain the boundary condition that $\delta w/(n + i\mathbf{k}\cdot\mathbf{u})$ is continuous across the TD, i.e.,

$$\frac{\delta w_i}{n + i\mathbf{k}\cdot\mathbf{u}_i} = \frac{\delta w_h}{n + i\mathbf{k}\cdot\mathbf{u}_h} = \zeta. \tag{18}$$

Next, from the perturbed continuity equation (Equation (13)), we obtain

$$\delta\rho = -\frac{n + i\mathbf{k}\cdot\mathbf{u}}{n - \nu_p/2\gamma + i\mathbf{k}\cdot\mathbf{u}}\frac{d\rho}{dz}\zeta. \tag{19}$$

The z component of Equation (14) is given by

$$\frac{d}{dz}\left(\delta p + \frac{\mathbf{B}\cdot\delta\mathbf{B}}{4\pi}\right) + \rho(n + \nu_p + \nu_s + i\mathbf{k}\cdot\mathbf{u})\delta w - \frac{(i\mathbf{k}\cdot\mathbf{B})\delta B_z}{4\pi} = \frac{(-\nu_p V_p\cos\theta - \nu_s V_s\cos\Psi)}{n - \nu_p/2\gamma + i\mathbf{k}\cdot\mathbf{u}}\frac{d\rho}{dz}\zeta, \tag{20}$$

where we have eliminated the perturbed plasma density from Equation (19) and we have used $V_{pz} = V_p\cos\theta$ and $V_{sz} = V_s\cos\Psi$. We now solve this equation across the singular surface at $z = 0$ and away from it and match the two solutions to obtain the eigenvalue, n.

1. *Solution across the singular surface*. In the neighborhood of the TD, we integrate Equation (20) across $z = 0$ from $+\varepsilon$ to $-\varepsilon$ and take the limit $\varepsilon \to 0$ to obtain

$$\left(\delta p + \frac{\mathbf{B}\cdot\delta\mathbf{B}}{4\pi}\right)_i - \left(\delta p + \frac{\mathbf{B}\cdot\delta\mathbf{B}}{4\pi}\right)_h = \frac{\rho_i - \rho_h}{2}\left[\frac{(-\nu_{pi}V_p\cos\theta - \nu_{si}V_s\cos\Psi)(n + i\mathbf{k}\cdot\mathbf{u}_i)}{n - \nu_{pi}/2\gamma + i\mathbf{k}\cdot\mathbf{u}_i} + \frac{(-\nu_{ph}V_p\cos\theta - \nu_{sh}V_s\cos\Psi)(n + i\mathbf{k}\cdot\mathbf{u}_h)}{n - \nu_{ph}/2\gamma + i\mathbf{k}\cdot\mathbf{u}_h}\right]\zeta, \tag{21}$$

where ε corresponds to the interstellar side and $-\varepsilon$ to the IHS side.

2. *Solution away from the singular surface*. Away from the singular surface, the density is assumed to be constant; hence, we neglect the last term in Equation (20) to obtain

$$\frac{d}{dz}\left(\delta p + \frac{\mathbf{B}\cdot\delta\mathbf{B}}{4\pi}\right) + \rho(n + \nu_p + \nu_s + i\mathbf{k}\cdot\mathbf{u})\delta w - \frac{(i\mathbf{k}\cdot\mathbf{B})\delta B_z}{4\pi} = 0. \tag{22}$$

A relation between δw and δB_z may be obtained by taking the z component of Equation (16) which gives

$$\left(\frac{\partial}{\partial t} + \mathbf{u}\cdot\nabla\right)\delta B_z = \mathbf{B}\cdot\nabla\delta w. \tag{23}$$

From this equation, we obtain the relation

$$\delta B_z = \frac{(i\mathbf{k}\cdot\mathbf{B})\delta w}{n + i\mathbf{k}\cdot\mathbf{u}} = (i\mathbf{k}\cdot\mathbf{B})\zeta. \tag{24}$$

The perturbed total pressure $\Phi = (\delta p + \mathbf{B}\cdot\delta\mathbf{B}/4\pi)$ in this region can be obtained by solving Poisson's equation:

$$\nabla^2\Phi = \frac{\partial^2\Phi}{\partial z^2} - k^2\Phi = 0. \tag{25}$$

Poisson's equation is obtained by neglecting the flow gradients and the perturbed density away from the singular surface in Equation (14), taking the divergence of the remaining equation and using $\nabla\cdot\delta\mathbf{u} = 0$ and $\nabla\cdot\delta\mathbf{B} = 0$. The solution of Φ on the two sides of the HP are $\phi \propto \exp(-kz)$ in the region $z > 0$ and $\phi \propto \exp(kz)$ in the region $z < 0$. Eliminating δw and δB_z in Equation (22) through Equations (18) and (24), and using the solution of Φ in the OHS and the IHS we get, respectively,

$$\left[\rho_h(n + \nu_{ph} + \nu_{sh} + i\mathbf{k}\cdot\mathbf{u}_h)(n + i\mathbf{k}\cdot\mathbf{u}_h) + \frac{(\mathbf{k}\cdot\mathbf{B}_h)^2}{4\pi}\right]\zeta = -k\left(\delta p + \frac{\mathbf{B}\cdot\delta\mathbf{B}}{4\pi}\right)_h, \tag{26}$$

$$\left[\rho_i(n + \nu_{pi} + \nu_{si} + i\mathbf{k}\cdot\mathbf{u}_i)(n + i\mathbf{k}\cdot\mathbf{u}_i) + \frac{(\mathbf{k}\cdot\mathbf{B}_i)^2}{4\pi}\right]\zeta = k\left(\delta p + \frac{\mathbf{B}\cdot\delta\mathbf{B}}{4\pi}\right)_i, \tag{27}$$

where B_i and B_h are the magnitudes of the interstellar and heliosheath magnetic fields in the vicinity of the HP. Matching the solution across the singular surface given in Equation (21) with the solution away from the singular surface finally gives the DR as

$$\left[\rho_h(n + \nu_{ph} + \nu_{sh} + i\mathbf{k}\cdot\mathbf{u}_h)(n + i\mathbf{k}\cdot\mathbf{u}_h) + \frac{(\mathbf{k}\cdot\mathbf{B}_h)^2}{4\pi}\right] + \left[\rho_i(n + \nu_{pi} + \nu_{si} + i\mathbf{k}\cdot\mathbf{u}_i)(n + i\mathbf{k}\cdot\mathbf{u}_i) + \frac{(\mathbf{k}\cdot\mathbf{B}_i)^2}{4\pi}\right] = \frac{(\rho_i - \rho_h)k}{2}\left[\frac{(-\nu_{pi}V_p\cos\theta - \nu_{si}V_s\cos\Psi)(n + i\mathbf{k}\cdot\mathbf{u}_i)}{n - \nu_{pi}/2\gamma + i\mathbf{k}\cdot\mathbf{u}_i} + \frac{(-\nu_{ph}V_p\cos\theta - \nu_{sh}V_s\cos\Psi)(n + i\mathbf{k}\cdot\mathbf{u}_h)}{n - \nu_{ph}/2\gamma + i\mathbf{k}\cdot\mathbf{u}_h}\right]. \tag{28}$$

The DR in Equation (28) is general and takes into account the effects of charge exchange interactions with primary neutrals from LISM and ENAs from the heliosheath, and plasma flows and magnetic fields in the IHS and OHS. It is quartic in n and thus there are either four real roots or two pairs of complex roots. Instability occurs if roots have positive real parts. We use Equation (28) to study the stability of a particular region of the HP by appropriately choosing the value of θ and Ψ, including the region where *Voyager 1* crossed the HP. Equation (28) may be simplified by transforming to the frame of one of the flows, such as the frame of the OHS flow so that $u_i = 0$ and $U = |u_i - u_h|$. To solve the DR, we express it in the following dimensionless form:

$$[(\lambda+\delta+i\mu\cdot\mathbf{U})(\lambda+i\mu\cdot\mathbf{U})+\alpha(\lambda+1)\lambda+(\mu\cdot\mathbf{A}_i)^2+(\mu\cdot\mathbf{A}_h)^2] = \frac{(\alpha-1)\mu}{2}\left(\frac{\lambda(-\cos\theta - f_1\cos\Psi)}{\lambda-1/2\gamma} + \frac{(-\delta\cos\theta - f_2\cos\Psi)(\lambda+i\mu\cdot\mathbf{U})}{\lambda+i\mu\cdot\mathbf{U}-\delta/2\gamma}\right), \quad (29)$$

where $\mathbf{A}_{i/h} = \mathbf{V}_{Ai/h}/V_p$, $\mathbf{V}_{Ai/h} = \mathbf{B}_{i/h}/\sqrt{4\pi\rho_h}$. The relative velocity $\mathbf{U}$ and the distance z are normalized as $U \equiv |\mathbf{u}_i - \mathbf{u}_h|/V_p$ and $z \equiv z/L$, where $L = V_p/\nu_{pi}$ is the charge exchange length scale for LISM neutrals and $\lambda = n/\nu_{pi}$, $\delta = \nu_{ph}/\nu_{pi}$, $\alpha = \rho_i/\rho_h$, and $\mu = \mathbf{k}V_p/\nu_{pi}$. The parameters f_1 and f_2 are defined as $f_1 = \nu_{si}V_s/\nu_{pi}V_p$ and $f_2 = \nu_{sh}V_s/\nu_{pi}V_p$. We have also neglected ν_{si} and ν_{sh} in comparison to ν_{pi} and ν_{ph} on the LHS of Equation (28) since $\nu_{si}/\nu_{pi} < 1$ and $\nu_{sh}/\nu_{ph} < 1$. Next, we examine the stability of various regions of HP using the DR (Equation (29)). Typical values of the plasma density and temperature in the IHS and OHS and neutral density in the nose and flanks region have been given above. Typical values of the neutral flow velocity, charge exchange frequencies, and magnetic fields, and ratio of plasma densities in the OHS and IHS are $V_p \simeq 20$ km s^{-1}, $V_s \simeq 100$ km s^{-1}, $\nu_{pi} \simeq 10^{-9}$ s^{-1}, $\nu_{ph} \simeq 10\nu_{pi} \simeq 10^{-8}$ s^{-1}, $\nu_{si} = 10^{-11} \simeq \nu_{sh}$, $B_i \simeq 3$ μG, $B_h \simeq 5$ μG and $\alpha \simeq 20$ (Borovikov et al. 2008; Zank et al. 2013).

1. *Nose region of the HP*. This region is characterized by weak plasma flows $U \simeq 0$ km s^{-1}, LISM neutral flow along $-z$ ($\cos\theta \sim -1$) and ENAs that are counter streaming along z, hence $\cos\Psi \simeq 1$. In this case, the DR (Equation (29)), which is fourth order in n, is given by

$$[(\lambda+\delta)\lambda+\alpha(\lambda+1)\lambda+(\mu\cdot\mathbf{A}_i)^2+(\mu\cdot\mathbf{A}_h)^2] = \frac{(\alpha-1)\mu}{2}\left(\frac{\lambda(1-f_1)}{\lambda-1/2\gamma}+\frac{(\delta-f_2)\lambda}{\lambda-\delta/2\gamma}\right). \quad (30)$$

   In this region, the plasma density gradient and the effective gravity due to primary LISM neutrals are in opposite directions hence the RT mode will be strongest. The counter streaming ENAs, magnetic field, and the ion–neutral collisions provide a stabilizing influence on the RT instability. In the absence of a magnetic field and ENAs, this DR reduces to the cubic DR originally obtained by Zank (1999a) and later by Florinski et al. (2005). The DR is solved for typical values of $\alpha = 20, \delta = 10, \gamma = 5/3$, $A_i = 10$, $A_h = 15$, and $f_1 \simeq f_2 \simeq 0.05$. Since f_1 and f_2 are small, the stabilizing influence of the ENAs can be expected to be weak. To see the effect of magnetic field stabilization, we first solve the DR for zero magnetic field $A_i = A_h = 0$. Figure 1 (top plot) shows the three roots in the absence of the magnetic field, of which two are unstable.

   These roots are similar to the one obtained earlier by Zank (1999a) and Florinski et al. (2005) in the absence of a magnetic field. Typical modes with wave lengths in the range 100–500 AU are unstable. In Figure 1 (bottom plot), we show four roots that include the effects of magnetic fields in the IHS and OHS.

   The plot shows a marginal reduction of the growth rate even when the unstable mode is propagating in the direction of the magnetic field, i.e., $\mathbf{A}\cdot\mu = A\mu$. In this case, the stabilizing influence of the magnetic field is strongest. The stabilization effect for other angles is weaker and zero for perpendicular propagation. We find that the stabilization is not complete even for very large values of the magnetic field. Typical values of the growth rates are $\lambda \simeq 1$–3, which for heliosphere parameters corresponds to a growth time of 50–100 yr. This time scale agrees with the time scale for the quasi-periodic oscillations of the nose seen in the numerical simulations of the HP (Florinski et al. 2005). Our results thus show that the nose region of the HP is unstable to RT-like modes with a growth time of roughly 50–100 yr with wavelengths ranging from 100–500 AU. The stabilizing influence of typical values of magnetic fields in the IHS and OHS and of ENAs is found to be weak in this region.
2. *Shoulder region of the HP*. This region is characterized by the simultaneous presence of a KH-like instability due to flow shear and the RT-like instability, though the latter is somewhat weakened as compared to the nose region because $|\cos\theta| < 1$. For our calculation, we choose $\theta = 135^\circ$ and $\cos\theta = -0.7$ while $\cos\Psi \simeq 1$. In the simulations of Borovikov et al. (2008) a typical value for the flow shear across HP is $U \simeq 2$. Values for the other parameters are the same as those given above. The DR has four roots for these parameters, which are shown in Figure 2. Two roots have positive real parts, thus indicating instability. The mixed KH–RT mode is a new form of instability driven by a combination of ENAs and primary neutrals, and is seen in the simulations of Borovikov et al. (2008).
3. *Flank region of the HP*. In this region, the LISM neutral flow (as well as the plasma flow) is along the x-direction, hence $\cos\theta = 0$. Since the plasma density gradient is along z, the RT drive is eliminated and LISM neutrals play no role in destabilizing the flanks (and can in fact act to damp a KH instability—Zank 1999a). However, ENAs now play an important role. The ENAs travel upstream nearly along z, hence $\cos\Psi \simeq 1$. Consequently, energetic neutrals can be expected to influence the KH instability on the flanks, which is caused by flow shear along z. The DR in this region is given by

$$[(\lambda+\delta+i\mu\cdot\mathbf{U})(\lambda+i\mu\cdot\mathbf{U})+\alpha(\lambda+1)\lambda+(\mu\cdot\mathbf{A}_i)^2 + (\mu\cdot\mathbf{A}_h)^2] = \frac{(\alpha-1)\mu}{2}\left(-\frac{f_1\lambda}{\lambda-1/2\gamma}-\frac{f_2(\lambda+i\mu\cdot\mathbf{U})}{\lambda+i\mu\cdot\mathbf{U}-\delta/2\gamma}\right). \quad (31)$$

To show the effect of magnetic fields and ENAs, we first solve the DR without ENAs ($f_1 = f_2 = 0$) for modes propagating parallel to the magnetic field. The DR is a quadratic equation

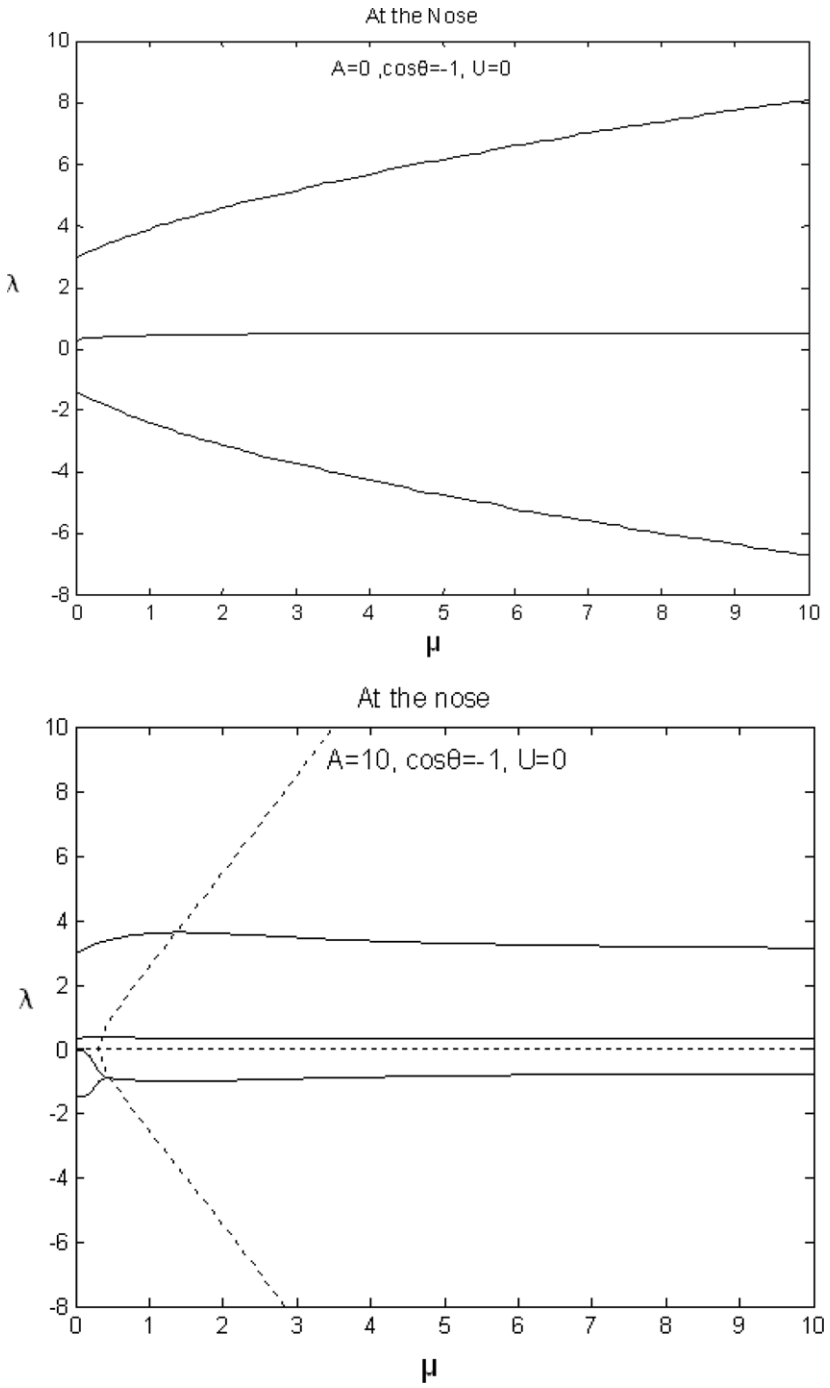

Figure 1. Top: the roots of the dispersion relation near the nose without magnetic field stabilization. The two roots with positive real parts show instability. Bottom: the roots of the dispersion relation near the nose with magnetic field. With a non-zero magnetic field, there are four roots instead of three. However, the stabilization of the unstable roots due to the magnetic field is marginal.

with two roots as shown in Figure 3 (top), both of which are stable. This is the KH instability, which is stabilized by magnetic fields. This behavior is consistent with the simulations of Borovikov et al. (2008), which show that in absence of ENAs the KH instability is stabilized by typical values of magnetic fields that are present in IHS and OHS. In Figure 3 (bottom), we show the roots when ENAs are included. There are unstable roots with positive real parts, which show that ENAs revive the instability of the flanks. Thus, in the presence of a magnetic field, ENAs are essential for driving an instability of the HP flanks. This behavior is consistent with the simulations of Borovikov et al. (2008).

4. NONLINEAR STABILITY

In the previous section, we have identified conditions under which the HP is linearly unstable to RT-like and/or KH-like instabilities. However, as the amplitude of the perturbation grows, nonlinear effects can become important, which may limit the growth of perturbations. Simulations of the global HP by Florinski et al. (2005) have shown that it exhibits quasi-periodic motion, returning to its previous configuration every 100 yr or so. This shows that nonlinear effects are indeed limiting the growth of the instability. There is vast body of analytic, numerical, and experimental literature on the nonlinear phases

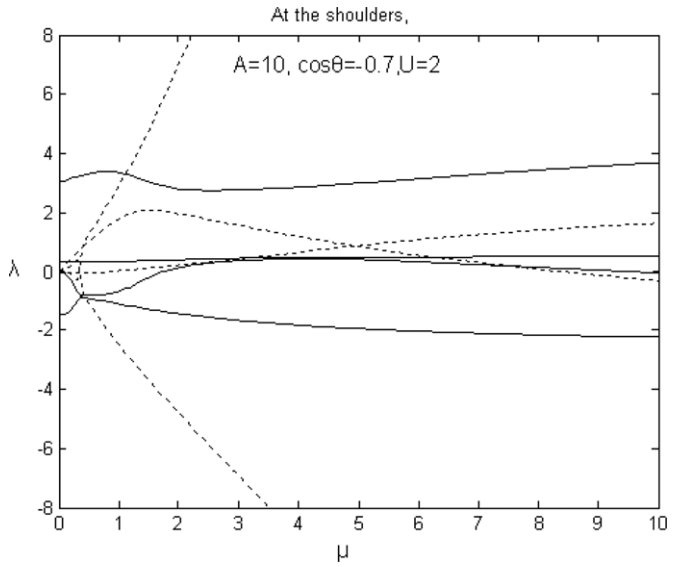

Figure 2. Roots of the dispersion relation in the shoulder region. The unstable roots correspond to mixed RT–KH modes. The dotted lines identify the imaginary part of the solution to the dispersion relation. The imaginary part of the solution shows that these are propagating modes.

of RT and KH instabilities (Castaing et al. 1980; Sohn 2004). In the general case, the linear perturbations of the RT instability develop into an exponential growth phase with bubbles of lighter fluid rising into the heavier fluid, and spikes of heavier fluid penetrating into the lighter fluid. This nonlinear state is characterized by Atwoods number $A = (n_h - n_l)/(n_h + n_l)$, where n_h and n_l are the densities of heavy and light fluids, respectively. For $A \leqslant 1$, falling spikes are seen to grow into mushroom-like structures. For $A \simeq 1$, the nonlinear state consists of freely falling spikes and constant velocity rising bubbles. The sides of the freely falling spikes may also be subject to a secondary KH instability. In the case of the HP with $\alpha = \rho_i/\rho_s \simeq 20$, $A = 0.9$, the nonlinear state will consist of growing mushrooms consistent with the simulations of Florinski et al. (2005) and Borovikov et al. (2008). However, unlike the general case, the mushroom-like structures cannot grow indefinitely in the case of the HP. As noted earlier (Florinski et al. 2005), there are two factors that inhibit the growth of perturbations: convection of the perturbation along the HP and the compressibility of the plasma and magnetic field in the IHS plasma between HP and TS. As can be seen from Figures 1 (bottom) and 2, the unstable perturbations have a finite imaginary part, hence, a finite phase velocity along the HP. The nose region is the region of maximum instability where the density gradient and effective gravity are aligned in the opposite direction. However, unstable perturbations are quickly convected out of this zone, thus limiting the growth due the RT instability. Also, as the denser plasma from the LISM invades the plasma in the IHS, the TS is pushed inward against the ram pressure of the upstream flow, which limits the growth of perturbations. The magnetic field in the IHS may also contribute to the incompressibility, thereby stabilizing the RT instability. The numerical simulations of Borovikov et al. (2008) have shown that irrespective of whether the OHS magnetic field is present or not, the presence of the IHS magnetic field is crucial for the stabilization of RT instability. As can be seen from the general DR given in Equation (29), the linear theory does not distinguish between the two magnetic fields, hence this must be a nonlinear effect. The magnetic field in the IHS

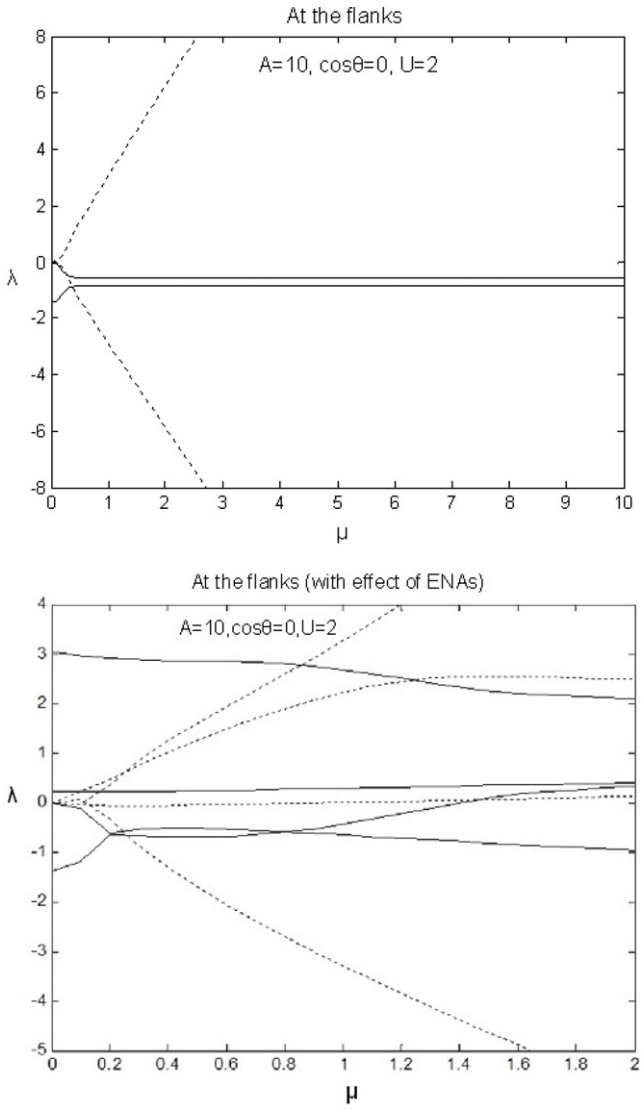

Figure 3. Top: the roots of the dispersion relation in the flank region with magnetic field but without ENAs. There are two roots and both are stable due to the stabilizing influence of the magnetic field. Bottom: the roots of the dispersion relation in the flank region with magnetic field and ENAs. The plot illustrates three unstable roots showing the destabilizing influence of ENAs on the KH modes.

will increase the compressibility of the plasma between the HP and TS, thereby inhibiting the growth of instability. The nonlinear evolution of the KH instability on the flanks could result in vortex formation in the saturation stage. However, in the case of the HP, the stabilization due to magnetic field tension and destabilization due to ENAs could result in large amplitude undulate structures without vortex formation. Such a nonlinear state without vortices is seen in the simulations of Borovikov et al. (2008). These nonlinear structures cause mixing of interstellar and solar plasma, which might be a source of soft X-ray emission in heliosheath (Robertson & Cravens 2003). As discussed by Florinski et al. (2005) the low frequency turbulence generated by these instabilities may also facilitate the propagation of galactic cosmic rays in the heliosphere.

5. SUMMARY AND DISCUSSION

To summarize, we have studied the stability of the HP. In an idealized view, it is a TD that separates the tenuous and hot heliosheath plasma from the relatively dense and cool plasma of

the LISM. In our model, we have included a number of effects that are important in the heliosphere, e.g., resonant change exchange between primary interstellar neutrals atoms and the SW plasma, interstellar and heliosheath magnetic fields, and plasma flows in the vicinity of the HP. We have also included the effects of ENAs or secondary hot neutrals from the IHS. These are generated as result of the charge exchange interaction of primary neutrals and hot heliosheath plasma. Recent numerical simulations of the global HP have shown that this population of neutrals plays a very significant role in the instability of the flanks of HP. Instead of using the full energy equation, we use Zank's charge exchange modified incompressibility condition (Zank 1999a) as the equation of state in our model. Under typical conditions, the plasma resistivity due to electron–neutral collisions, electron–ion collisions, or turbulence (anomalous) is found to be small, hence, the interstellar magnetic field drapes around the HP causing a north–south asymmetry. Due to the lack of symmetry, the stability analysis is carried out in a local reference frame located on the HP. The HP stability is studied in three regions. The nose region, where plasma flows are weak and unstable to RT-like modes, the shoulder region, unstable to mixed RT–KH-like modes, and the flank region (with strong flow and flow shear) which is unstable to a KH-like instability. Our derived DR shows that in the relevant parameter space, the nose region is RT unstable, driven by primary neutrals, with a growth rate of about 50–100 yr. In the shoulder region, a mixed RT–KH-like mode is unstable and is driven by a combination of effective gravity due to primary neutrals and plasma flow shear. In these regions, the effect of magnetization and ENAs is weak. However, magnetization and ENAs become effective in the flank regions where the impact of primary neutrals is weak as the effective gravity is perpendicular to plasma density gradient. In this region, in the absence of ENAs, the magnetic field parallel to the flow completely stabilizes the KH instability. In the presence of ENAs, the KH modes are destabilized. Thus, ENAs are essential for destabilization of the flanks in the presence of magnetic fields. These results are consistent with numerical simulations of Borovikov et al. (2008). In the case of the RT instability, the nonlinear state is characterized by Atwoods number A. If A is $\leqslant 1$, then the nonlinear state is characterized by the formation of mushroom-like structures, where the heavy fluid invades the lighter fluid (Castaing et al. 1980; Sohn 2004). The mushroom-like structures are seen in the numerical simulations of Florinski et al. (2005) and Borovikov et al. (2008). However, in the present case the growth of these structures is inhibited by convection out of the unstable zone and the compressibility of plasma and the magnetic fields in IHS. The nonlinear state of the KH instability, due to tension of magnetic fields, is characterized by the formation of undulating structures without vortices. These structures are expected to cause intermixing of interstellar and SW plasmas.

The hot neutrals or ENAs created in the IHS play an interesting role in the stability of the HP. For the RT instability, they have a stabilizing influence because close to the nose region they stream counter to the primary neutrals thereby weakening the effective gravity. For the KH instability, they have a destabilizing influence, and in the presence of magnetic field, are essential for the instability on the flanks.

Before concluding, we briefly relate the work presented here to that discussed by Fahr et al. (1986). Fahr et al. investigated plasma mixing across the HP boundary, and treated the HP as an extended transition layer. Much of the focus of their work is on electrostatic instabilities and HP structure and associated plasma mixing. However, Fahr et al. do briefly discuss the possibility of fluid instabilities. The temporal SW was regarded as a potential driver of RT and KH instabilities. By introducing an ad hoc acceleration term into the classical RT and KH DRs (Chandrasekhar 1981) to model time-varying SW conditions, Fahr et al. found that the HP could be driven unstable under some circumstances. However, they noted that unless the OHS and IHS magnetic fields were precisely oriented (so that the **k** vector is oriented perpendicularly to both the IHS and OHS **B** vectors), magnetic fields would always suppress fluid instabilities. Simulations of the interaction of the temporal SW with the LISM in the absence of magnetic fields (Zank & Müller 2003) did not reveal an HP that was subject to RT instabilities driven by solar cycle effects. Related three-dimensional MHD simulations that incorporate the time dependence of the SW by Washimi et al. (2011) also do not reveal an unstable HP. In the work of Fahr et al. (1986), however, the role of charge exchange in possibly driving these instabilities was never considered. In this regard, aside from superficial similarities, the analysis presented here is quite different from that discussed by Fahr et al. The recent simulations of a time-dependent SW driver coupled to the Zank (1999a) charge-exchange instability by Borovikov & Pogorelov (2014) show that indeed the HP can be highly unstable in these circumstances.

Let us consider what the effect might be of an instability on the HP that drags a loop of interstellar magnetic field (colored blue) into the IHS—Figures 4 and 5. At the nose and shoulder regions of the HP, the latter being the current location of *Voyager 1*, the RT element of the instability described here will drag a loop of magnetic field through the HP into the IHS. If we adopt a frame of reference that is comoving with the interstellar flow adjacent to the local HP, then the magnetic field lines on the interstellar side of the HP are fixed. The initial loop is illustrated in Figure 4(i). The flow in the IHS is faster than in the VLISM and has both a northward and westward component as viewed from the Sun. As the VLISM magnetic field protrudes into the IHS, it is dragged in a corresponding direction (relative to the VLISM flow) with the footpoints remaining anchored to the same relative locations on the HP. The dragged and distorted interstellar magnetic field is shown in Figure 4(i) by the dashed blue line. The interplanetary field (colored red) in the IHS can be oriented in one or the other direction as illustrated in Figure 4 or Figure 5, depending on the sector boundary structure ahead of the HP. Interplanetary magnetic field that was below the interstellar loop protruding into the IHS will be pushed up against the loop as it is dragged (more slowly) by the IHS flow. As illustrated in Figure 4(i), part of the dragged loop of VLISM magnetic field will be anti-parallel to the IHS magnetic field that is pushing up against it. These sections of the VLISM and IHS magnetic fields can experience reconnection, with the resulting reconfigured field lines (now red and blue) illustrated in Figure 4. No island-like structures are expected to form, but, instead, one part of the IHS magnetic field connects to the VLISM magnetic field that returns to the VLISM. The other section of the IHS magnetic field connects to the VLISM magnetic field that is entering the IHS from the ISM. The IHS flow will tend to straighten the recently reconnected magnetic field, yielding a final configuration similar to that shown in Figure 4(iii). The key points are that (1) one of the field lines allows direct access from the IHS to the VLISM, and thus allows direct access of energetic heliospheric particles to the ISM, and the other magnetic field line allows direct access of energetic galactic particles from the VLISM into the IHS; and (2) the magnetic field structure

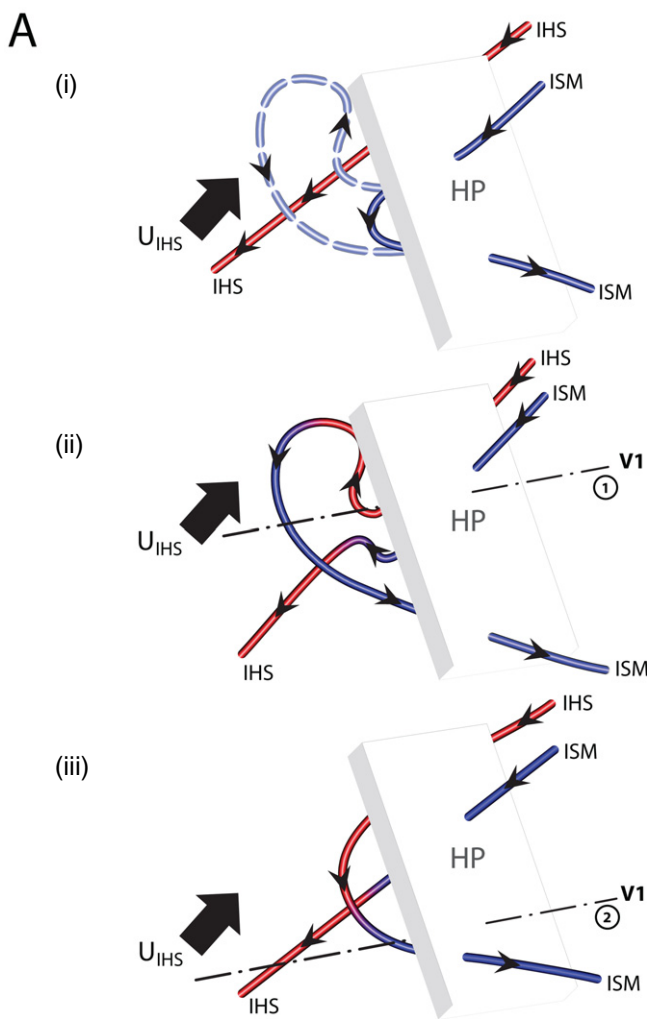

Figure 4. Cartoon showing the possible evolution of an OHS/VLISM magnetic field line dragged into the IHS by either an RT-like or mixed KH–RT-like instability on the HP. For convenience, we have assumed that we are in the stationary frame of the OHS flow. The red line shows the IHS magnetic field. In this example, we suppose that the IHS and OHS magnetic field lines are approximately parallel to one another on either side of the HP (sketched as the shaded block and labeled HP). The heavy black arrow depicts the IHS plasma flow direction as measured in the frame of the OHS flow. (i) The solid blue line depicts the initial incursion of the OHS magnetic field dragged into the IHS by an RT-like instability. The dashed blue line shows the later OHS magnetic field line after being dragged northward and westward (assuming we are considering the approximate location of *Voyager 1*) by the IHS plasma flow. The IHS magnetic field (red line) is convected northward and westward by the IHS plasma flow. (ii) As the IHS magnetic field line is advected in the IHS plasma flow, it will eventually be forced against the intruding OHS magnetic field line, which in the OHS plasma flow frame of reference is anchored to the HP. Because the OHS magnetic field has been dragged as illustrated in (i), there will always be a region that is anti-parallel to the impinging IHS magnetic field. In this region, as illustrated, the IHS and OHS magnetic field lines can reconnect. In so doing, the entering OHS magnetic field line is connected to an IHS magnetic field section, thereby allowing direct access of OHS plasma into the IHS. Conversely, the other segment of the IHS magnetic field is now connected to the OHS magnetic field, thereby allowing direct access of IHS plasma into the OHS. (iii) After some time, the magnetic field connecting the IHS to the OHS and vice versa will be dragged into the parallel configuration illustrated here. The dash-dotted lines, labeled A1 and A2, depict possible *Voyager 1* trajectories through the magnetic field line topologies and HP. In Figure 6, we illustrate possible changes in the azimuthal angle that might be observed by *Voyager 1* for the trajectories shown.

(A color version of this figure is available in the online journal.)

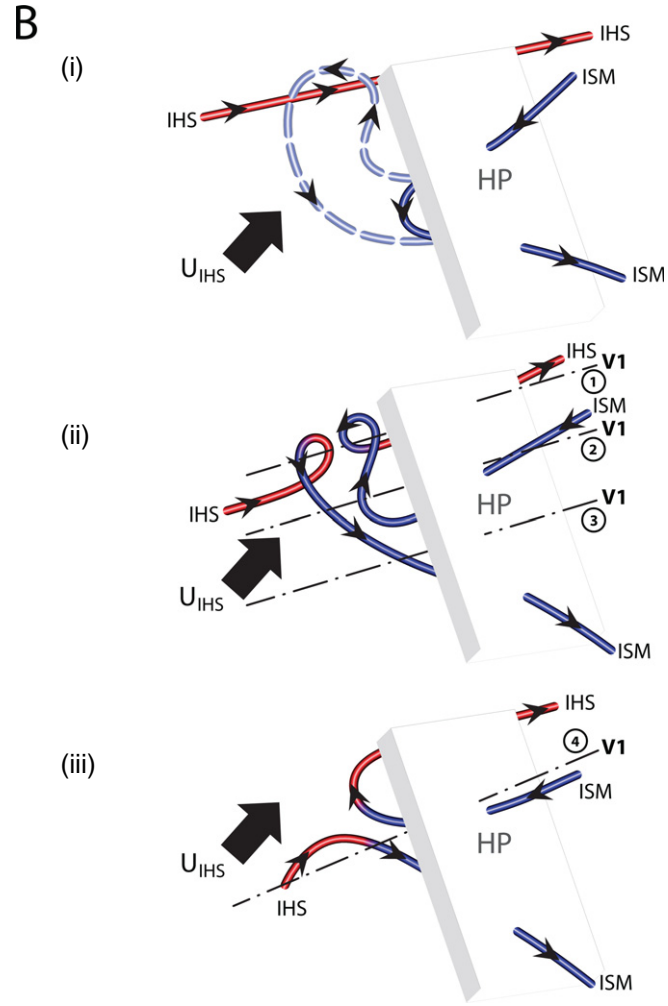

Figure 5. Same as Figure 4 except that the IHS is now oriented anti-parallel to the OHS magnetic field. Four possible *Voyager 1* trajectories have been sketched, B1–B4. As illustrated in Figure 4, the net result is that again the IHS and OHS magnetic fields reconnect and allow the exchange of plasma from IHS to OHS and vice versa.

(A color version of this figure is available in the online journal.)

on either side of the HP is unlikely to be very complicated. To illustrate the last point, we sketch sample *Voyager 1* trajectories through the HP and plot in Figure 6 sample azimuthal angle λ profiles. The most complicated profile yields some three sector boundary-like changes, whereas the simplest reveals no changes and at best a gradual change in λ.

Illustrated in Figure 5 is a corresponding set of figures showing the possible evolution of an interstellar loop protruding into the IHS, but now with an IHS magnetic field directed oppositely to that of Figure 4. A similar reconnection event between the dragged distorted loop of VLISM magnetic field and the IHS magnetic field pushing up from below yields an similar laminar magnetic field structure in which one part of the IHS field is connected to the VLISM magnetic field that re-enters the ISM, and the other to the VLISM magnetic field that enters the IHS. As before, azimuthal angle plots (Figure 6) for sample *Voyager 1* trajectories in Figures 5(ii) and (iii) suggest the presence of at most a few sector boundary-like changes or perhaps only one. The reconnected magnetic field line topology yields again easy loss of energetic heliospheric particles and entrance of galactic energetic particles. In some respects, the scenario described above may be similar to the suggestion made by Schwadron & McComas (2013) that *Voyager 1* may have found itself in a flux transfer event, which would have a similar magnetic field configuration between IHS and OHS.

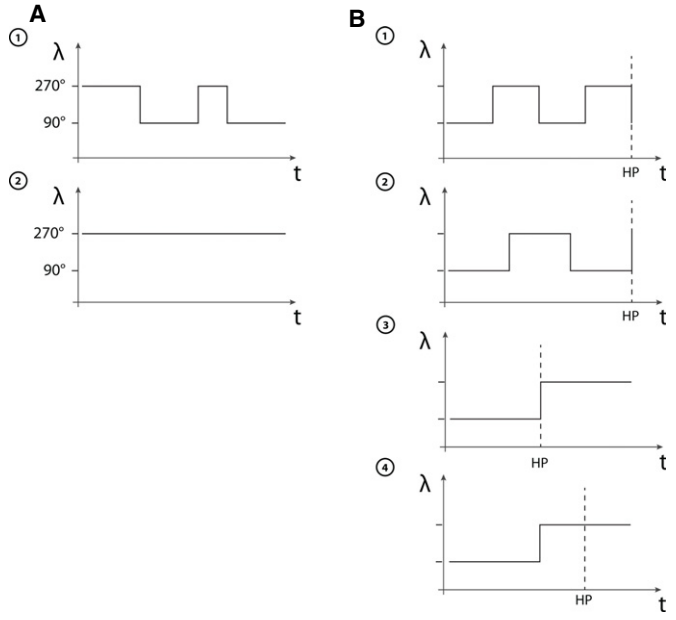

Figure 6. Graphs showing the temporal variation in the azimuthal angle λ that might be expected for the various *Voyager 1* trajectories (dash-dotted lines) illustrated in Figures 4 (A1 and A2) and 5 (B1–B4).

The form of the reconnected IHS and VLISM magnetic field described above is an explanation for the observed galactic and anomalous cosmic ray behavior seen by *Voyager 1*. Furthermore, since the magnetic field configuration holds for either orientation of the IHS magnetic field, we believe that this explanation is quite robust. We note that Borovikov & Pogorelov (2014) suggest that solar cycle variation might provide the perturbation to initiate the Zank instability. It is also possible that the highly dynamical state of the IHS described by Zank & Müller (2003) and Washimi et al. (2011) will perturb the HP and thus drive instabilities.

As illustrated in the cartoon Figures 4 and 5, the mixing of interstellar and solar plasmas is likely to be efficient in the neighborhood of an instability. This has interesting implications for the emission of soft X-rays in the heliosphere (Florinski et al. 2005). The high atomic number SW ions in the SW plasma can charge exchange with neutrals in the hydrogen wall giving rise to enhanced soft X-ray emission (Cravens 1997; Cox 1998). A simplified form of this possibility was simulated by Borovikov et al. (2008).

This work was supported by NASA grant NNX10AC17G and IBEX NASA/SwRI award NNG05EC85C, subcontract A99132BT. Discussions with V. Florinski, J. Heerikhuisen, and N. Pogorelov are gratefully acknowledged. G.P.Z. appreciates discussions at the team meeting "Heliosheath Processes and Structure of the Heliopause: Modeling Energetic Particles, Cosmic Rays, and Magnetic Fields" supported by the International Space Science Institute in Bern, Switzerland.

REFERENCES

Baranov, V. B., Fahr, H. J., & Ruderman, M. S. 1992, A&A, 261, 341
Baranov, V. B., & Malama, Y. G. 1993, JGR, 98, 15,157
Ben-Jaffel, L., Strumik, M., Ratkiewicz, R., & Grygorczuk, J. 2013, ApJ, 779, 130
Borovikov, S. N., & Pogorelov, N. V. 2014, ApJL, 783, L16
Borovikov, S. N., Pogorelov, N. V., Zank, G. P., & Kryukov, I. A. 2008, ApJ, 682, 1404
Burlaga, L. F., Ness, N. F., Gurnett, D. A., & Kurth, W. S. 2013, ApJL, 778, L3
Castaing, B., Gunarante, G., Heslot, F., et al. 1980, JFM, 204, 1
Chalov, S. V. 1994, P&SS, 42, 55
Chandrasekhar, S. 1981, Hydrodynamic and Hydromagnetic Stability (New York: Dover)
Cox, D. P. 1998, in IAU Colloq. 166, The Local Bubble and Beyond, ed. D. Breitschwerdt, M. J. Freyberg, & J. Truemper (Berlin: Springer), 121
Cravens, T. E. 1997, GeoRL, 24, 105
Dasgupta, B., Florinski, V., Heerikhuisen, J., & Zank, G. P. 2006, in AIP Conf. Proc. 858, Physics of the Inner Heliosphere, ed. J. Heerikhuisen et al. (Melville, NY: AIP), 51
Ershkovich, A. I., & Mendis, D. A. 1983, ApJ, 269, 743
Fahr, H. J., Neutsch, W., Grzcdzielski, S., Macek, W., & Ratkiewicz, R. 1986, SSRv, 43, 329
Florinski, V., Zank, G. P., & Pogorelov, N. V. 2005, JGR, 110, A07104
Gruntman, M. 1992, P&SS, 40, 439
Gruntman, M., Roelof, E. C., Mitchell, D. G., et al. 2001, JGR, 106, 15767
Gurnett, D. A., Kurth, W. S., Burlaga, L. F., & Ness, N. F. 2013, Sci, 341, 1489
Heerikhuisen, J., Florinski, V., & Zank, G. P. 2006, JGR, 111, A06110
Heerikhuisen, J., & Pogorelov, N. V. 2011, ApJ, 738, 29
Heerikhuisen, J., Pogorelov, N. V., Florinski, V., Zank, G. P., & le Roux, J. A. 2008, ApJ, 682, 679
Holzer, T. E. 1972, JGR, 77, 5407
Ichimaru, S. 1973, Basic Principle of Plasma Physics; A Statistical Approach (New York: Benjamin)
Liewer, P. C., Karmesin, S. R., & Brackbill, J. U. 1996, JGR, 101, 17119
Lindsay, B. G., & Stebbings, R. F. 2005, JGR, 110, A12213
Malama, Y. G., Izmodenov, V. V., & Chalov, S. V. 2006, A&A, 445, 693
Pauls, H. L., Zank, G. P., & Williams, L. L. 1995, JGR, 100, 21595
Robertson, I. P., & Cravens, T. E. 2003, JGRA, 108, 6
Ruderman, M. S. 2000, Ap&SS, 274, 327
Ruderman, M. S., Brevdo, L., & Erdélyi, R. 2004, RSPSA, 460, 847
Schwadron, N., & McComas, D. 2013, ApJL, 778, L33
Sohn, S.-I. 2004, PhRvE, 69, 036703
Strumik, M., Ben-Jaffel, L., Ratkiewicz, R., & Grygorczuk, J. 2011, ApJL, 741, L6
Washimi, H., Zank, G. P., Hu, Q., et al. 2011, MNRAS, 416, 1475
Zakharian, A. R., Webb, G. M., & Zank, G. P. 1998, in AIP Conf. Proc. 471, Solar Wind 9, ed. S. R. Habbal et al. (Melville, NY: AIP), 799
Zank, G. P. 1999a, in AIP Conf. Proc. 471, Solar Wind Nine, ed. S. R. Habbal et al. (Melville, NY: AIP), 783
Zank, G. P. 1999b, SSRv, 89, 413
Zank, G. P., Heerikhuisen, J., Pogorelov, N. V., Burrows, R., & McComas, D. 2010, ApJ, 708, 1092
Zank, G. P., Heerikhuisen, J., Wood, B. E., et al. 2013, ApJ, 763, 20
Zank, G. P., & Matthaeus, W. H. 1991, PhFl, 3, 69
Zank, G. P., & Müller, H.-R. 2003, JGR, 108, 1240
Zank, G. P., Müller, H.-R., & Wood, B. E. 2001, PhPl, 8, 2385
Zank, G. P., Pauls, H. L., Williams, L. L., & Hall, D. T. 1996, JGR, 101, 21639